EFFECT OF PHASE- AND TEMPERATURE-DEPENDENT STRAIN-HARDENING SLOPES ON THE CALCULATED WELDING RESIDUAL STRESSES IN S235 STEEL

J. SUN*, T. NITSCHKE-PAGEL*, K. DILGER*

**Technische Universität Braunschweig, 38106 Braunschweig, Germany*

10.3217/978-3-85125-968-1-17

ABSTRACT

The purpose of this work is to systematically clarify the impact of phase- and temperature-dependent strain-hardening slopes on the calculated welding residual stresses in the commonly used structural steel S235. Both experimental methods and numerical simulation have been utilized for investigation. The results reveal that the temperature-dependent strain-hardening slopes of the generated phases (austenite and bainite here) have nearly no influence on the simulated welding residual stresses. The calculated magnitude of longitudinal residual stress in the base metal near the weld area is highly sensitive to the applied strain-hardening slopes of the initial microstructure (ferrite here), while that of transverse residual stress is not. Meanwhile, comparing to the strain-hardening slope of the initial microstructure at elevated temperatures, that at room temperature plays a critical role in the simulated longitudinal residual stress. In this study, the guidance on how to economically and reliably determine the temperature- and phase-dependent strain-hardening slopes of a given steel in numerical welding simulation is provided.

Keywords: Strain-hardening slopes; Structural steel S235; Numerical simulation; Welding residual stresses.

INTRODUCTION

Arc welding has been widely used to join steels in manufacturing industries because of its low-cost equipment and portability [1]. Nevertheless, the extremely inhomogeneous temperature field is formed during arc welding due to the highly localized arc energy input. The shrinkage of the heated zone is strongly hindered by the surrounding cold area [2]. As a consequence, residual stresses are unavoidably generated in the weldments [3, 4]. It is well known that the tensile residual stress might reduce the fatigue strength [5]. Therefore, it is of critical significance to accurately predict the magnitude and distribution of residual stresses for the assessment of structural integrity of welded components.

With the enhancement of computing technology and computational welding mechanics (CWM), numerical simulation using the finite element method (FEM) becomes a reliable,

economical, and efficient alternative to obtain the magnitude and distribution of welding residual stresses [4, 6]. In comparison to the experimental methods often requiring a considerable amount of cost, time, and effort, numerical simulation has been drawn increasing attention from manufacturing industries.

During arc welding, the steel near the molten area experiences a plastic compression-tension yielding [3]. Based on the measured stress-strain curves of the widely used steels, it can be found that the commonly applied steels in practice usually show the obvious strain-hardening phenomenon [7-8]. Therefore, it is necessary to carefully consider strain-hardening phenomenon in numerical welding simulation. If the strain hardening effect is taken into account in numerical welding simulation, three very important aspects should be carefully considered: strain-hardening model, strain-hardening recovery, and strain-hardening slope [9]. Until now, great effort has been made to clarify which strain-hardening model is the best for a given steel in numerical welding simulation and to study the mechanism of strain-hardening recovery [9-10]. However, there is less literature to illustrate the effect of strain-hardening slope on the calculated welding residual stresses. It is well known that the strain-hardening slope might be not only temperature but also phase dependent. How to economically and reliably determine the temperature- and phase-dependent strain-hardening slopes of a given steel in numerical welding simulation is currently unclear.

As fundamental research, the numerical sensitivity analyses based on Sysweld software have been conducted to illuminate how the strain-hardening slopes are economically and reasonably determined for the accurate prediction of residual stresses in S235 steel weldments. Meanwhile, the mechanical tensile tests were performed to measure the stress-strain curves at different temperatures. The welding experiments were carried out to measure the temperature results and residual stresses for validation.

EXPERIMENTAL PROCEDURE

The base metal (BM) is the structural steel S235JR. The measured stress-strain curves of the given steel S235JR at various temperatures are shown in Fig. 1. The tungsten inert gas (TIG) arc welding was applied to produce the single-pass weldment without the addition of a filler wire. The designed size of the weld plate is 200 × 150 × 10 mm as seen in Fig. 2. The applied welding current is 200 A, welding voltage is 12.5 V, and welding speed is 10 cm/min.

Before welding, thermocouples were arranged on the top surface of the weld specimen for measuring the temperature history. After welding, the X-ray diffraction method was applied to measure the welding residual stresses. The macrograph at the transverse mid-cross section were measured by using the optical microscope.

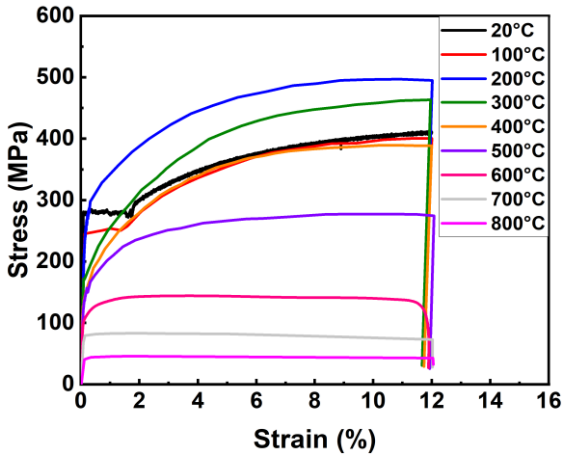

Fig. 1 Measured stress-strain curves at different temperatures of base plate

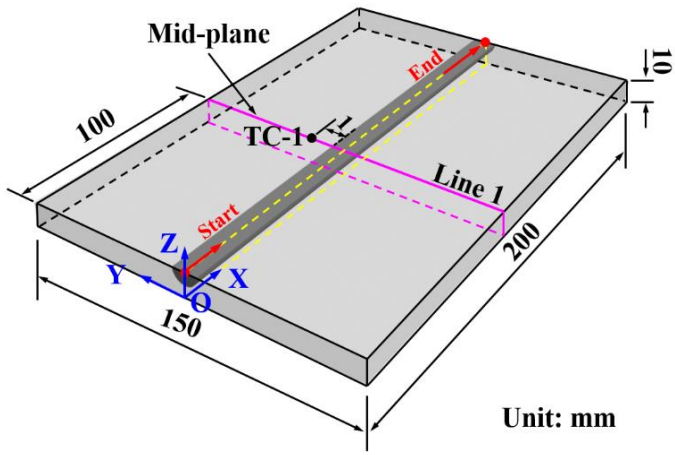

Fig. 2 Designed geometry of the weld specimen

FINITE ELEMENT ANALYSIS

The created FE mesh model can be seen in Fig. 3. The size of the FE model is completely the same as that of the experimental weld sample (see Fig. 2). The finer meshes were designed in and near the weld, while the coarser meshes were applied in the area away from the weld. In the present work, the subsequently coupled thermo-metallurgical-mechanical FEM was applied for numerical welding simulation here.

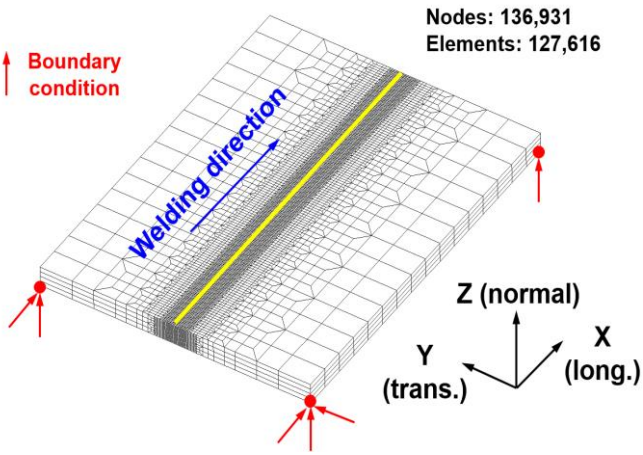

Fig. 3 Created finite element model

THERMAL ANALYSIS

Goldak's double ellipsoidal heat source was used to simulate the arc energy input here [11]. The used thermal properties of the given structural steel S235JR can be seen in [10]. The fusion zone (FZ) was assumed to be the area with peak temperature higher than 1500 °C, while the temperature range of the heat-affected zone (HAZ) was between 750 and 1500 °C [10]. The heat transfer caused by the thermal conduction was calculated based on Fourier rule. The heat loss induced by heat convection (q_c) and radiation (q_r) was considered according to Newton's law and Stefan-Boltzmann law, respectively.

METALLURGICAL ANALYSIS

In the present study, the austenization start (Ac1) and end (Ac3) temperature were set as 730 and 860 °C, respectively [10]. The applied continuous-cooling-transformation (CCT) diagram for the given steel S235JR here as seen in Fig. 4 refers to that of S235 steel provided by Loose [12]. In the current work, the diffusive phase transformation from austenite to ferrite/pearlite/bainite was calculated according to the Leblond kinematic rule. The displacive phase transformation from austenite to martensite was simulated based on the Koistinen-Marburger (KM) relationship model. Furthermore, the linear mixture rule was utilized to determine the material properties of the phase mixture [10].

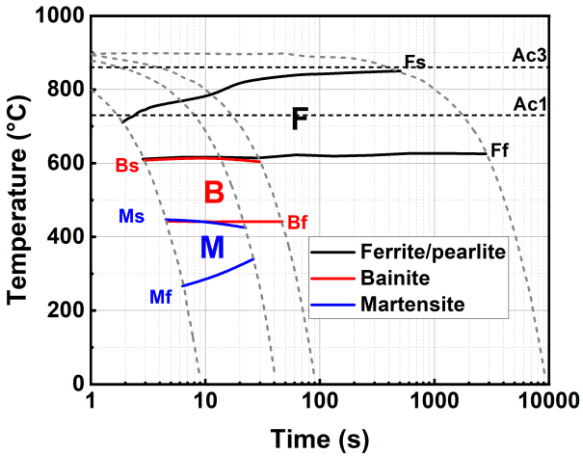

Fig. 4 Continuous-cooling-transformation diagram of S235 steel (refer to [12])

MECHANICAL ANALYSIS

The utilized mechanical properties of the given steel S235JR steel here can be found in [10]. The strain-hardening slopes of austenite, bainite, and martensite were taken from that in S235J2G3 steel included in the Simufact.welding material database, while that of ferrite were obtained from the experimental results as seen in Fig. 5 [10]. Note that the material properties of ferrite and pearlite in steels are usually assumed to be the same.

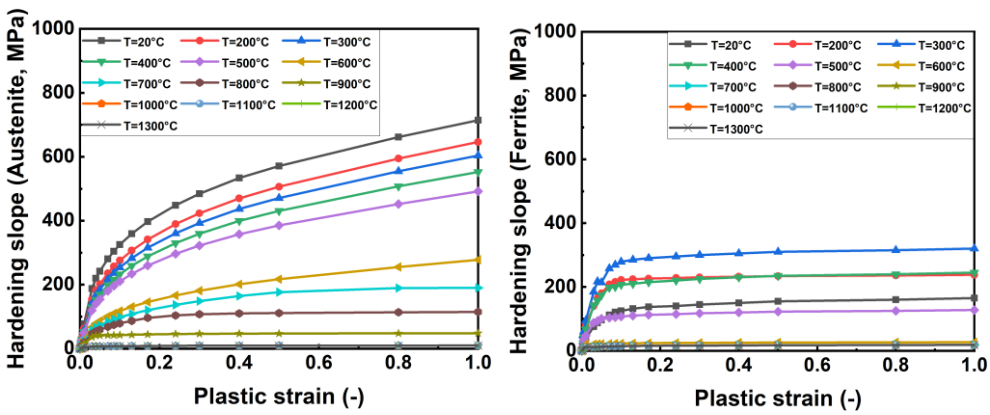

(a) Austenite (b) Ferrite/ Pearlite

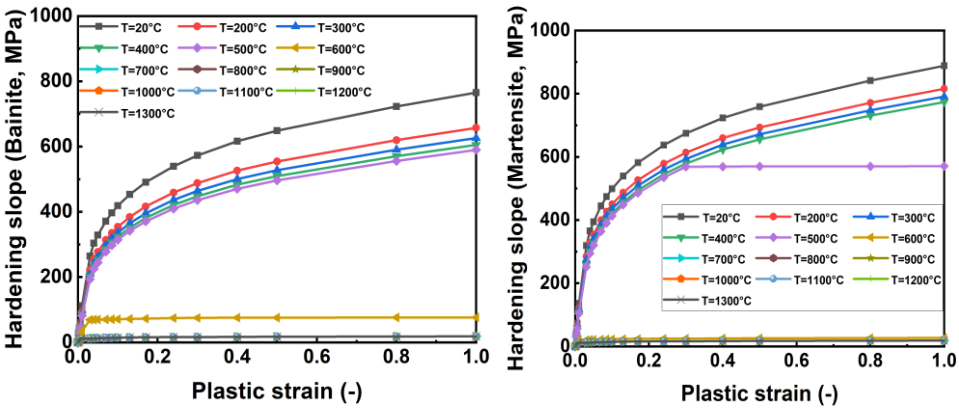

(c) Bainite (d) Martensite

Fig. 5 Strain-hardening slopes of S235 steel

SIMULATION CASES

In this study, the cases in Table 1 were elaborately designed and performed using Sysweld software for studying the effect of strain-hardening slope on welding residual stresses. The isotropic hardening model was employed and the annealing temperature was set as 860 °C (Ac3) for all the cases in Table 1 [10]. Note that all these cases are the same except the employed strain-hardening slopes. Here, cases A-1 and B-1are identical and considered to be the standard case. The "Fig.5 (No change)" in Table 1 means the strain-hardening slopes are equal to that in Fig.5.

Table 1 Simulation cases

Cases		Strain-hardening slope
Group A	Case A-1	Fig. 5 (No change)
	Case A-2	Austenite·5 times
	Case A-3	Bainite·5 times
	Case A-4	Ferrite·5 times
Group B	Case B-1	Fig. 5 (No change)
	Case B-2	All temperatures: Ferrite·5 times
	Case B-3	All temperatures except T_{RT}: Ferrite·5 times
	Case B-4	Only T_{RT}: Ferrite·5 times

In Group A, the effect of the phase-dependent strain-hardening slopes on the calculated welding residual stresses was systematically investigated. The strain-hardening slopes of only one of the phases in each case were changed, while the rest were kept as the same as that in the standard case. For example, just all the temperature-dependent strain-hardening slopes of ferrite simultaneously were highly increased 5 times in Case A-4. Since almost no martensite is generated in the weldment after welding based on the measured thermal results as seen later, the variation in the strain-hardening slopes of martensite was not

investigated here. In Group B, the impact of the temperature-dependent strain-hardening slopes of S235 steel base metal (ferrite) on the calculated welding residual stresses was systematically studied. Here, the strain-hardening slope of ferrite at different temperatures was changed. For instance, the strain-hardening slopes of ferrite at all temperatures were increased 5 times in Case B-2, while that only at room temperature T_{RT} were increased 5 times in Case B-4.

RESULTS AND DISCUSSION

WELDING TEMPERATURE FIELD

Since the subsequently coupled FEM was employed in numerical simulation and only the strain-hardening model as well as slope in the mechanical analysis were changed here, it can be expected that the calculated welding temperature fields in all these cases in Table 1 are nearly the same. For this reason, the calculated welding temperature field in Case A-1 is taken as an example for comparison with the experimental results.

Fig. 6 compares the calculated and measured weld dimension in the transverse mid-cross section. From this figure, it can be found that the calculated sizes of FZ and HAZ match the experimental results very well. Fig. 7 shows the predicted and measured thermal cycles at the TC-1 location (see Fig. 2). In Fig. 7, the simulated cooling rate $\Delta t_{8/5}$ time is in good agreement with the experimental data. According to the above comparisons, it can be concluded that the current thermal analysis is reliable and can provide the reasonable welding temperature field.

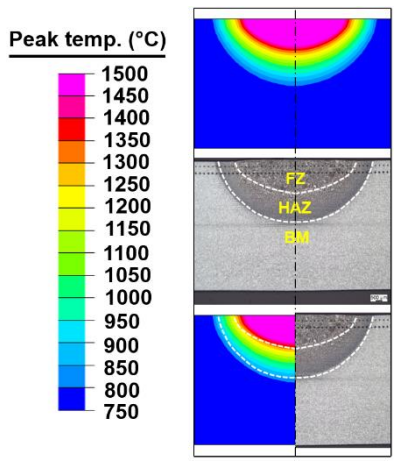

Fig. 6 Peak temperature distribution

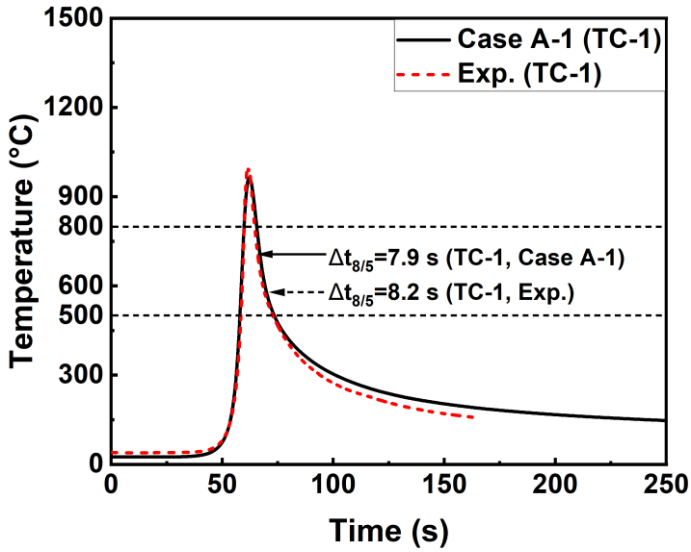

Fig.7 Thermal cycles at TC-1 location

WELDING RESIDUAL STRESSES

Longitudinal residual stress

Fig. 8 depicts the longitudinal residual stress distribution along line 1 simulated by the cases in groups A and B. In Fig. 8a, the calculated results along line 1 in case A-1, A-2, and A-3 are nearly the same. Nevertheless, the predictions in Case A-4 are different from that in the other three cases mainly in the base metal near the weld area. This is due to that solid-state phase transformation (SSPT) mainly occurs in the weld area, which nearly eliminates the strain-hardening effect [9]. In Fig. 8b, the predictions in Case B-1 and Case B-3 are nearly the same. That in Case B-2 and Case B-4 are almost identical. Nevertheless, the calculated results in Case B-1 is quite different from that in Case B-2 mainly in the base metal near the weld area.

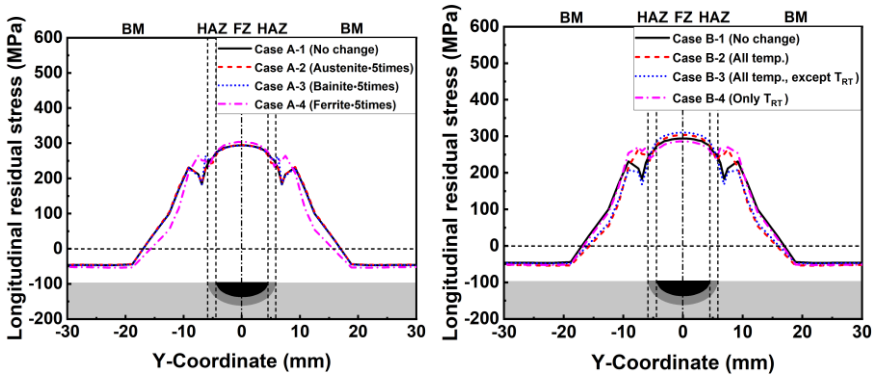

(a) Cases in Group A (b) Cases in Group B

Fig. 8 Predicted longitudinal residual stress distribution along line 1 in cases of groups A and B

Fig. 9 shows the longitudinal residual stress distributions along line 2 calculated by the cases in groups A and B. From Fig. 9a, it can be seen that the calculated results in the weld area in these cases are nearly the same, while that in the base metal near the weld area in Case A-4 are much higher than that in the other three cases. In Fig. 9, the predictions in the base metal very close to the weld area in Case A-3 is a little higher than that in Case A-1 or Case A-2. Furthermore, the calculated results in the weld area in Case A-2 are slightly different from that in the other three cases. This is because the austenite exists before SSPT but then fades away after SSPT, while the bainite arises and remains after SSPT. Meanwhile, partial SSPT occurs at the border area of HAZ. It should be noted that these slight differences are induced by the high increase in the strain-hardening slopes of austenite and bainite fivefold here. In Fig. 9b, the predictions in Case B-1 and Case B-3 are very close, which is different from that in Case B-2 and Case B-4. The calculated results in Case B-4 is quite similar to that in Case B-2 overall.

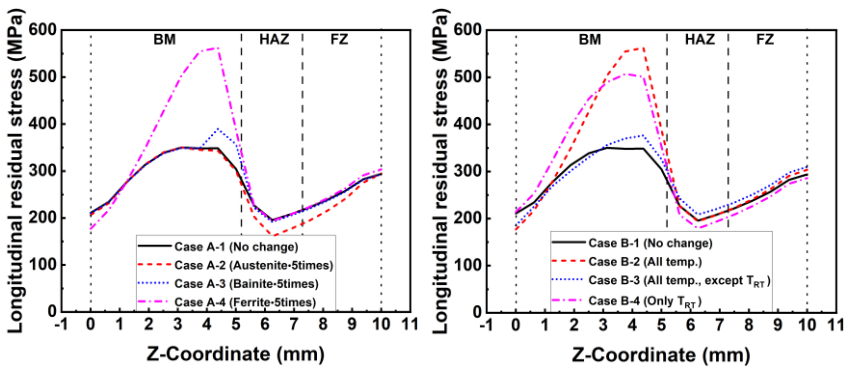

(a) Cases in Group A (b) Cases in Group B

Fig. 9 Predicted longitudinal residual stress distribution along line 2 in cases of groups A and B

Transverse residual stress

Fig. 10 presents the simulated transverse residual stress distribution along line 1 in cases of groups A and B. From Fig. 10, one can see that the calculations are nearly the same except a certain difference in base metal very close to the weld area.

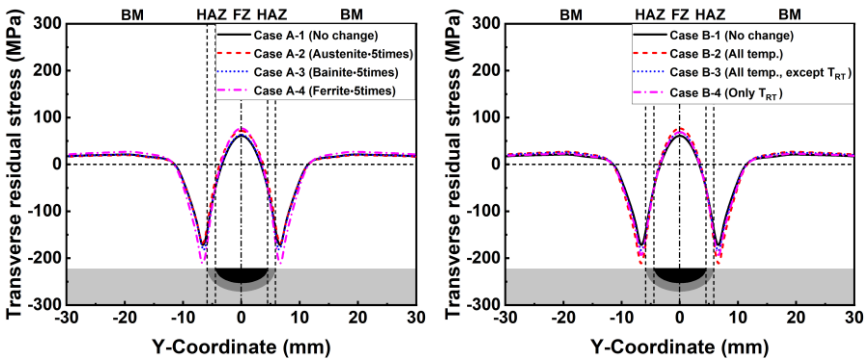

(a) Cases in Group A (b) Cases in Group B

Fig. 10 Predicted transverse residual stress distribution along line 1 in cases of groups A and B

Fig. 11 depicts the transverse residual stress distribution along line 2 simulated by the cases in groups A and B. From Fig. 11a, one can see that the calculations in Case A-1, Case A-2, and Case A-3 are nearly the same, which are different from that in Case A-4 mainly in the base metal near the weld area. However, it should be mentioned that the difference in the calculated magnitude of transverse residual stress in the base metal near the weld area between Case B-4 and Case B-1 (or Case B-2, Case B-3) is rather low. Furthermore, this small deviation is obtained by highly increasing the strain-hardening slopes of ferrite fivefold here. In Fig. 11b, the predictions in Case B-1 and Case B-3 are nearly the same. That in Case B-2 and Case B-4 are similar. Nevertheless, the calculated results in Case B-1 is slightly different from that in Case B-2 mainly in the base metal near the weld area.

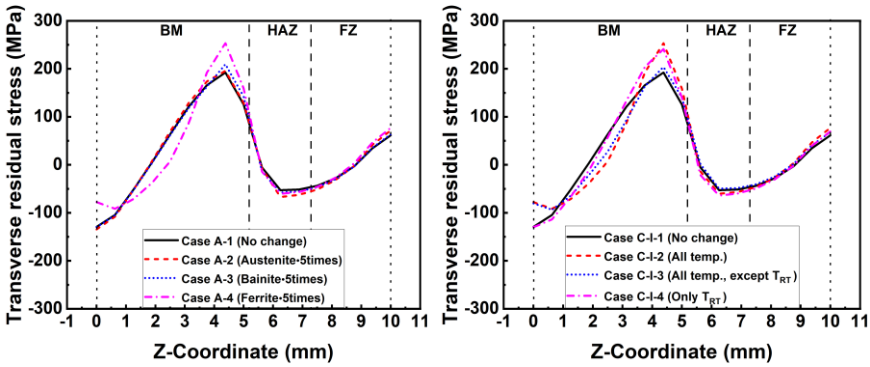

(a) Cases in Group A (b) Cases in Group B

Fig. 11 Predicted transverse residual stress distribution along line 2 in cases of groups A and B

CONCLUSIONS

(1) The variations in the strain-hardening slopes of the generated phases (austenite and bainite here) have nearly no effect on the calculated welding residual stresses.
(2) The calculated magnitude of longitudinal residual stress in the base metal near the weld area is highly sensitive to the applied strain-hardening slopes of the initial microstructure (ferrite here), while that of transverse residual stress is nearly not.
(3) In comparison to the strain-hardening slopes of the parent microstructure at elevated temperatures, that at room temperature plays a critical role in the predicted longitudinal residual stresses.
(4) Guidance on how to economically and reliably determine the phase- and temperature-dependent strain-hardening slopes of a given steel in numerical welding simulation is provided.

APPENDICES AND ACKNOWLEDGEMENTS

The authors are grateful for the financial support provided by the German Research Foundation “Deutsche Forschungsgemeinschaft (DFG)” through the projects NI 508/14-2 and SU 1411/1-1 for the present research.

References

[1] J. GRANJON: *Fundamentals of welding metallurgy*, Cambridge, 2002.
[2] TH. NITSCHKE-PAGEL and H. WOHLFAHRT: ‘Residual stresses in welded joints – sources and consequences’, *Master. Sci. Forum* Vol. 404, pp. 215-226, 2002.
[3] D. RADAJ: *Heat effects of welding on temperature field, residual stress and distortion*, Berlin-Heidelberg, 1992.

[4] Y. UEDA, H. MURAKAWA and N. MA: *Welding deformation and residual stress prevention*, Berlin-Heidelberg, 2012.
[5] TH. NITSCHKE-PAGEL and J. HENSEL: 'An enhancement of the current design concepts for the improved consideration of residual stresses in fatigue-loaded welds', *Welding in the world*, Vol. 65, pp. 643-651, 2021.
[6] L. LINDGREN: *COMPUTATIONAL WELDING MECHANICS*, CAMBRIDGE, 2007.
[7] Nickel Institution: The Nickel Advantage – Nickel in stainless steel – Eurometaux, 2008.
[8] M. FARAJIAN: 'Welding residual stress behavior under mechanical loading'. *Welding in the world*, Vol. 57, pp. 157-169, 2013.
[9] J. SUN, J. HENSEL, J. KLASSEN, TH. NITSCHKE-PAGEL and K. DILGER: 'Solid-state phase transformation and strain hardening on the residual stresses in S355 steel weldments', *Journal of material processing technology*, Vol. 265, pp. 173-184, 2019.
[10] J. SUN, TH. NITSCHKE-PAGEL, K. DILGER: 'Influence of strain-hardening models and slopes on the predicted residual stresses in strcutural steel S235 weldments', *Journal of materials research and technology*, Vol. 19, pp. 4044-4062, 2022.
[11] J. GOLDAK: *Computational welding mechanics*, Springer, 2005.
[12] T. LOOSE: *Einfluß des transienten Schweißvorganges auf Verzug Eigenspannungen und stabilitätsverhalten axial gedrückter Kreiszylinderschalen aus Stahl*, thesis, Karlsruhe: Universität Fridericiana zu Karlsruhe, 2007.